Geophysical Journal International

Geophys. J. Int. (2024) **240,** 1009–1027
Advance Access publication 2024 November 29
GJI Seismology

https://doi.org/10.1093/gji/ggae425

Reconciling the irreconcilable: window-based versus stochastic declustering algorithms

I. Spassiani,[1] S. Gentili,[2] R. Console,[1,3] M. Murru,[1] M. Taroni[1] and G. Falcone[1]

[1] *Istituto Nazionale di Geofisica e Vulcanologia (INGV), Via di Vigna Murata* 605, 00143 *Rome, Italy. E-mail: ilaria.spassiani@ingv.it*
[2] *National Institute of Oceanography and Applied Geophysics - OGS, Borgo Grotta Gigante 42/c,I-34010 Sgonico(Trieste), Italy*
[3] *Center of Integrated Geomorphology for the Mediterranean Area, 85100 Potenza, Italy*

Accepted 2024 November 21. Received 2024 November 21; in original form 2024 April 2

SUMMARY

Short-term earthquake clustering is one of the most essential features of seismicity. Clusters are identified using various techniques, generally deterministic and based on spatiotemporal windowing. Conversely, the leading approach in short-term earthquake forecasting has a probabilistic view of clustering, usually based on the epidemic type aftershock sequence (ETAS) models. The effectiveness of the deterministic techniques and whether or not to prefer a probabilistic approach is often debated in the literature: sharp cutoffs or randomness degree? In this study, we contribute to the debate by "measuring" (inferring) seismic clusters, identified by two different deterministic window-based techniques, in terms of the ETAS probabilities associated with any event in the clusters, to investigate the consistency between deterministic and probabilistic approaches. Inference is performed by considering, for each event in an identified cluster, the corresponding probability of being independent and the expected number of triggered events according to ETAS. Results show no substantial differences between the two deterministic cluster identification procedures, and an overall consistency between the identified clusters and the relative events' ETAS probabilities. A consistency between probabilistic and deterministic declustering approaches is also important for seismic hazard analyses, where the latter approach is routinely used for its simplicity.

Key words: Statistical methods; Earthquake dynamics; Earthquake interaction, forecasting, and prediction.

1 INTRODUCTION

The epidemic type aftershock sequence (ETAS) model represents a benchmark in statistical seismology, very often used to forecast earthquake sequences at various spatiotemporal scales (Ogata 1998; Console & Murru 2001; Console *et al.* 2003, 2007; Lombardi & Marzocchi 2010; Omi *et al.* 2014). It is a branching, self-exciting Hawkes process, according to which any seismic event may generate its own aftershocks independently of the other events and the background ("spontaneous", independent) ones. The ETAS model is based on four simple constitutive laws, that is, (i) the Omori–Utsu for the aftershocks' temporal decay, (ii) a spatial distribution usually of Gaussian type, (iii) the exponential Gutenberg–Richter law for the events' frequency magnitudes, and (iv) the productivity law for the expected number of aftershocks generated by an event with a given magnitude (Omori 1895; Gutenberg & Richter 1944; Utsu 1957; Ogata 1988, 1998; Zhuang *et al.* 2002). This model specifically provides the conditional intensity function, which completely represents the point process of earthquakes occurrences in a fixed space–time–magnitude domain.

One key strengths of ETAS relies on its capability to account for the main characteristic of seismicity, that is, events' clustering in space and time. Due to its probabilistic nature, the ETAS model is often used to decluster an earthquake catalogue through a stochastic approach. However, it is important to stress that a stochastic declustered catalogue is not unique, as it depends on the random numbers used to identify the events that constitute the background component of seismicity (Zhuang *et al.* 2002). Indeed, precisely because of its probabilistic nature, selecting a specific probability threshold to identify clusters using ETAS leads to a distortion of the hypothesis upon which this model is built. Instead, the cluster identification procedures typically adopted in the literature rest on deterministic window-based methods, according to which some constitutive equations are selected to set up the spatiotemporal extent of any cluster. Several different window-based methods have been proposed in the literature, mainly differing on the specific set of equations adopted (e.g. Gardner & Knopoff 1974; Keilis-Borok *et al.* 1980; Uhrhammer 1986; Zaliapin *et al.* 2008; van Stiphout *et al.* 2012).

Recent studies have investigated some classification similarities and differences between different clustering determination techniques, including both the stochastic earthquake declustering (SD) (Zhuang *et al.* 2002) and other window-based clustering methods like the nearest-neighbour (NN) approach (Zaliapin & Ben-Zion 2013). Spatiotemporal statistical measures and tools from network analysis are used by Varini *et al.* (2020) to prove that SD and NN produce similar partitions of the seismic catalogue into background events and earthquake clusters, but their topological structure could be different, especially in terms of complexity. Different declustering algorithms are performed and compared to investigate the spatiotemporal features of background seismicity in several catalogues worldwide, like for example in Benali *et al.* (2023) and Nas *et al.* (2019), where Monte Carlo simulations and tests are applied to show that, both SD and a modification of the method by Uhrhammer (1986), perform better than other methods to remove time clustering structures in Northern Algeria (Benali *et al.* 2023) and Turkey (Nas *et al.* 2019). A Markov Chain Monte Carlo mixture model is instead implemented in Bayliss *et al.* (2019) to create a new probabilistic approach to categorizing nearest neighbour event pairs aimed at constructing distinct seismic clusters, whose nature is then examined. A new probabilistic measure of clustering is finally proposed by Talbi *et al.* (2013) to rate different declustering algorithms according to their reference background model, to make possible comparing approaches based on different hypotheses and modelling. In practice, all these studies compare sets of clusters identified by deterministic and probabilistic techniques: the clustering structure is first identified by means of the different approaches, then the comparison is performed.

In this work, we do not set a probabilistic threshold to construct clusters stochastically. Unlike the papers above, we specifically detach ETAS from clustering identification. Instead, we compare the independence probability and expected number of descendants (aftershocks), that the ETAS model associates with any event in the seismic catalogue, to the clustering structure into which these events are deterministically (with probability 1) organized. In other words, we first identify clusters by applying only window-based techniques. Then, we develop an automatic approach based on two simple checks to assess whether the probabilities of each event being independent or triggered according to the ETAS model coherently reflect the structure of the identified clusters. We aim to interpret the deterministic results from a probabilistic perspective, providing new insights into the effectiveness of window-based techniques and determining whether a probabilistic method might be preferable.

It is worth mentioning that window-based models construct clusters starting from a strong event, usually named the "mainshock", and they occasionally merge more clusters. In contrast, in the ETAS model, events are not labelled as "mainshocks, aftershocks or foreshocks". ETAS just assigns to every event a probability of being background (independent) or triggered (dependent). Also in light of this difference, it is interesting to investigate whether and how the window-based clustering structure complies with the events' independence ETAS probabilities.

The specific formulation of the ETAS rate density we consider in this paper is given in Section 3 (see also Console *et al.* 2010). To (deterministically) identify clusters, we use instead a specific module of the software NESTORE v1.0 (Gentili *et al.* 2023), which allows the user to define the spatiotemporal laws describing the clusters' extent. As we will explain in Section 4.1, we will consider here the sets of laws by Gardner & Knopoff (1974), mostly used in the literature, and those by Uhrhammer (1986) and Lolli & Gasperini (2003), like in Gentili & Di Giovambattista (2017). As we will see, these two models will lead to similar results and will both be better at identifying dependent events than independent ones.

Eventually, window-based declustering algorithms are routinely used in probabilistic seismic hazard analysis (PSHA), because of their straightforward applications also in the case of historical seismic catalogues, where the completeness is not uniform with time and space. In such catalogues, the more sophisticated declustering methods based on ETAS are hardly applicable. However, Mizrahi *et al.* (2021) clearly show that window-based declustering algorithms lead to a biased estimation of the Gutenberg–Richter b-value parameter (Gutenberg & Richter 1944), a fundamental parameter for PSHA. This bias does not exist if the seismic catalogue is declustered with a stochastic approach. An effective solution to this problem is to use the window-based declustered catalogue for the spatial estimation of the seismicity, and the complete (i.e. not declustered) catalogue for the b-value estimation (Marzocchi & Taroni 2014). A consistency between probabilistic and deterministic declustering approaches will then better justify this practical solution, suggested by Marzocchi & Taroni (2014) and applied in some recent PSHA studies (e.g. the national PSHA model for New Zealand, Gerstenberger *et al.* 2023).

2 THE EARTHQUAKE CATALOGUE

The earthquake catalogue we consider in this study is ISIDe (Italian Seismological Instrumental and Parametric Data-Base, http://terremoti.ingv.it/ISIDe) including data from 2005 April 18 to 2021 April 30 over the entire Italian territory and some neighboring areas covered by the Italian seismic network (see panel a) of Fig. S1 in the Supplemental Material. The minimum and maximum magnitudes in the catalogue are ML 0.9 and ML 6.1, respectively. The completeness threshold estimated for this catalogue by Zhuang *et al.* (2019) is ML 2.9; the incremental and cumulative magnitude distributions are given in Fig. 1; in the Supplemental Material we also include a more detailed analysis to justify the choice of this threshold by means of the Lilliefors test (see panels b and c of Fig. S1, Supporting Information; Marzocchi *et al.* 2020; Herrmann & Marzocchi 2021). We count 5084 events in the ISIDe catalogue above the completeness magnitude, which we name "I-events" hereafter.

3 THE SPATIOTEMPORAL ETAS MODEL

The ETAS model we adopt to perform our analysis can be represented by a conditional intensity function in the form:

$$\lambda(t,x,y,m|H_t) = f_r\lambda_0(x,y,m) + \sum_{\{k:t_k<t\}} H(t-t_k)\lambda_k(t,x,y,m),$$

where

$$\lambda_k(t,x,y,m) = \kappa(m_k)g(t-t_k)f(x-x_k,y-y_k|m_k)f(m|m_k)$$

is the kernel function for the triggered seismicity, $\lambda_0(x,y,m)$ is the background intensity function assumed to be independent of time, f_r is the fraction of spontaneous over the total number of events (failure rate), $H(\cdot)$ is the step function, and $g(t)$, $f(x,y|m_k)$ and $f(m|m_k)$ are the response functions (i.e. probability density functions), respectively for the occurrence time, spatial location and magnitude of events triggered by an ancestor (parent event) with magnitude m_k.

The magnitude distribution for background events is independent of location and identical to that of their offspring (Zhuang *et al.* 2002). Under these conditions, the model's conditional intensity

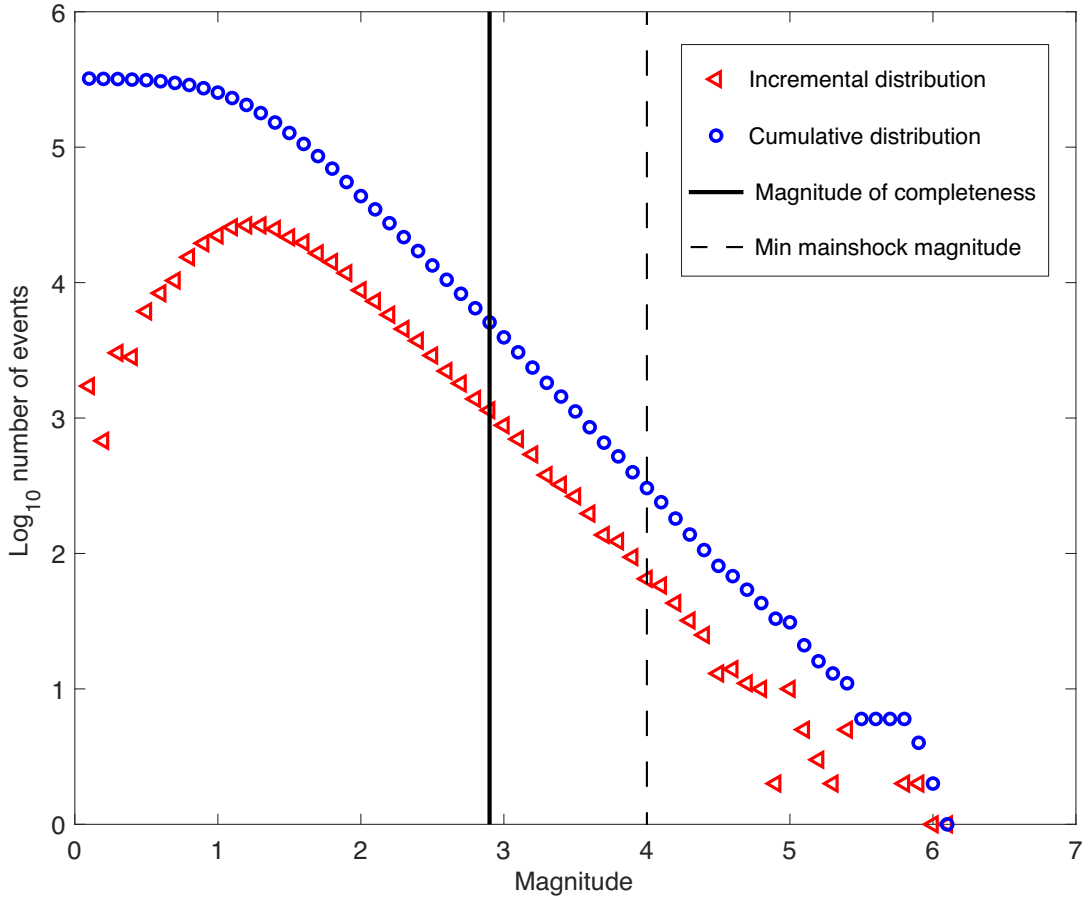

Figure 1. Incremental (triangles) and cumulative (circles) magnitude distributions of the events in the ISIDe earthquake catalogue considered in this study (time window: 2005 April 18 – 2021 April 30). The completeness magnitude ML 2.9 and the minimum magnitude for a mainshock to generate a cluster ML 4.0 are also represented as continuous and dashed black lines, respectively.

function can be decomposed as

$$\lambda(t, x, y, m|H_t) = f(m)\lambda(t, x, y|H_t),$$

where

$$\lambda(t, x, y|H_t) = f_r\lambda_0(x, y) + \sum_{\{k:t_k<t\}} H(t - t_k)\kappa(m_k)g(t - t_k) f(x - x_k, y - y_k|m_k).$$

The fact that the k-th event excites a non-stationary Poisson process with intensity $\kappa(m_k)g(t - t_k)f(x - x_k, y - y_k|m_k)$ indicates that $\kappa(m_k)$ represents the expected number of aftershocks (descendants) generated by an ancestor with magnitude m_k. In our specific case, the spatiotemporal

kernel function for the triggered seismicity is explicitly given by

$$K\left[\frac{d_i^2}{(x - x_i)^2 + (y - y_i)^2 + d_i^2}\right]^q (t - t_i + c)^{-p},$$

where $d_i = d_0 10^{\alpha(m_i - m_0)/2}$ and $(K, d_0, q, c, p, \alpha)$ are free, positive parameters typically estimated through the maximum likelihood estimation (MLE) technique.

In order to assess the consistency between the deterministically determined clusters and the ETAS stochastic measures (Console & Murru 2001; Console *et al.* 2003), we will associate to any I-event both the corresponding ETAS probability of being independent, and the number of descendants expected by the ETAS model. The first quantity is obtained as the ratio between the rate density of the background events and the total rate density (Zhuang *et al.* 2002); the second quantity is instead simply the expected average number of triggered shocks per each event. More precisely, let us assume that the seismic events are chronologically numbered from 1 to N. The probability that event j is triggered by event i can be estimated naturally as the relative contribution of event i to the

occurrence rate at the time and location of event j:

$$\rho_{ij} = \frac{\kappa(m_i)g(t_j - t_i)f(x_j - x_i, y_j - y_i|m_i)}{\lambda(t_j, x_j, y_j, m_j)}.$$

The probability for the event j to be an offspring is then $\rho_j = \sum_{i=1}^{j-1} \rho_{ij}$. Similarly, the probability for this event j being a background is

$$\phi_j = 1 - \rho_j = \frac{f_r\lambda_0(x_j, y_j)}{\lambda(t_j, x_j, y_j)}.$$

The expected number of descendants (aftershocks) of a parent event is finally computed by summing the expected rate of aftershocks it produces, over all the previous events in the catalogue. This is expressed by the function

$$n_j = \sum_{k=1}^{j-1} \kappa(m_k)g(t_j - t_k)f(x_j - x_k, y_j - y_k|m_k),$$

where m_k is the magnitude of the parent event. The number of descendant events can be zero if the parent event is not followed by any aftershocks, emphasizing the importance of both the theoretical model and the observed seismic behaviour in determining aftershock productivity.

To explicitly obtain these stochastic measures, we use the algorithms developed by Console *et al.* (2010) with the parameters estimated by means of the MLE technique, which is performed over the entire earthquake catalogue considered here (see Section 2). The parameter values found in the last iteration are $(f_r, K, d_0, q, c, p, \alpha) = (0.25, 0.12, 1.18, 1.89, 5.7\text{ E-}03, 1.09, 0.54)$. The choice of not considering space–time varying parameters is to be coherent with the window-based methods, for which we use fixed equations for the entire territory, as we will explain in Section 4.1.

4 CLUSTER IDENTIFICATION METHODS

Most window-based cluster identification methods have a similar algorithm. They start from an equation defining the spatiotemporal triggering area for the mainshock, set a minimum threshold for the mainshock magnitude and define the cluster of a mainshock m_i as "the set of all the earthquakes after m_i within its triggering area". If the cluster of a given mainshock contains a larger earthquake m_j, the clusters of m_i and m_j are merged, m_j becomes the cluster's mainshock and the events before m_j become foreshocks. The space window is a circular area around the mainshock, and the radius of the circle depends on the cluster identification method: different equations may be applied also depending on the seismotectonic of the region; both the radius and the time window are generally a function of the mainshock magnitude (van Stiphout *et al.* 2012).

4.1 The two approaches used to identify clusters

Here, we perform cluster identification by using a module implemented in the package NESTOREv1.0 (Gentili *et al.* 2023). This package allows us to detect clusters of seismicity by choosing the equations that define the space and time triggering area. In addition, it selects as foreshocks all the events before the mainshock within a radius arbitrarily set to 1.5 the radius of the mainshock, and a time window of 1 month. However, we will not take into account the foreshocks, to avoid possible multiple assignments of the same events to clusters close in space and time. For clarity, we stress that a cluster must contain at least two events. The two specific sets of equations we use to identify clusters are those by Uhrhammer (1986) – Lolli & Gasperini (2003) and by Gardner & Knopoff (1974) (respectively, "ULG-clusters" and "GK-clusters" hereafter; explicit formulas are given in Appendix A and graphed in Fig. S2 of the Supplemental Material). We will also set the threshold $M_m = 4.0$ as the minimum magnitude for a mainshock to generate its cluster. This specific choice is because, in Italy, there is a high percentage of background (i.e. random) events, and in the case of mainshocks smaller than 4.0, the window-based methods more likely fail to assign seismicity induced by the redistributed stress, that is the "true" aftershocks; they assign instead the events that occur there by chance.

4.2 Identification of ULG- and GK-clusters and their inference in terms of the ETAS independence probability

4.2.1 ULG-case

Implementing the ULG method in NESTOREv1.0 allowed us to identify 79 clusters above the completeness magnitude ML 2.9 (hereafter, ULG-clusters), with a minimum threshold for mainshock magnitude equal to 4.0. The number of events recognized as belonging to one of these clusters is 2516; since the cardinality (i.e. the total number of events) of the ISIDe catalogue is 5084, this means that there are 2568 "single" events, not associated with any ULG-cluster. Table S1 of the Supplemental Material lists some metrics of the ULG-clusters with the strongest magnitude ML 4.5+ (22 in total), such as the number of events and the first, last and strongest shocks involved. An interesting fact to point out is that there are some cases of temporal overlapping. For the sake of conciseness, the metrics of the remaining clusters are not reported, as these are considered less informative. In Fig. S3 of the Supplemental Material, we finally show all the ULG-clusters in different colours.

The 2568 I-events that do not belong to any ULG-cluster (hereafter, "unclustered-ULG") are mapped in panel (a) of Fig. 2, where they are coloured according to their independence ETAS probability. This makes it possible to compare individual events deterministically identified as being independent (unclustered) with their probability of being independent as an output of the best-fitting ETAS model. Panels (c) and (e) in the same figure concern instead the 2516 clustered events and all the 5084 events together, respectively. Clustered events are much more gathered than the unclustered-ULG ones.

The inset in panel a) of Fig. 2 shows the histogram of the independence probabilities associated with the events in no ULG-cluster, with (arbitrary) 0.1-bin length. The prevalence of unclustered-ULG events are observed in the bins $[0, 0.1]$ and $(0.9, 1]$, precisely 76 per cent of the total number, highlighting such events to have either a very high or a very low probability of being independent. Since we are focusing on the events not assigned to any ULG-cluster, the high bar of the histogram at the bin $(0.9, 1]$ is not a surprise. As regards the "very likely triggered" unclustered-ULG events, i.e., those with probability < 0.1, they are even a little more in number. Indeed, this group likely includes the events triggered by the foreshocks we excluded in the clustering identification procedure (see Subsection 4.1). Therefore, they are labeled as "non-independent" by ETAS, but there is no cluster's mainshock to which they are assigned. The great majority (97.4 per cent) of clustered events eventually have a very low probability of being independent (< 0.1), with the exception of a few of them reasonably representing the clusters' mainshocks. This is shown in panel c) of Fig. 2 and in the histogram of the relative inset.

The results just discussed are confirmed when considering a smaller bin-length, and are corroborated by the maps in top and middle panels of Fig. 3, where we plot separately the events with independence probability ≤ 0.1, ≤ 0.9 & > 0.1, > 0.9 (respectively in left, middle and right panels; blue color for the ULG case). In Fig. 3 we also indicate the relative percentages, together with the number of events considered and the sums of their expected descendants and independence ETAS probabilities. These quantities are summarized in Table S2 of the Supplemental Material. The inset in panel (e) of Fig. 2 and the bottom panels in Fig. 3 show the same results relative to all the events in the ISIDe catalogue.

4.2.2 GK-case

The GK-clusters identified by implementing the NESTOREv1.0 software with eqs (A2) of Appendix A are 82 in total. Their plot is given in Fig. S4 of the Supplemental Material. Again, we are considering the completeness magnitude ML 2.9 and the minimum threshold for mainshock magnitude equal to 4.0. In Table S3 of the Supplemental Material we also report some metrics relative to the

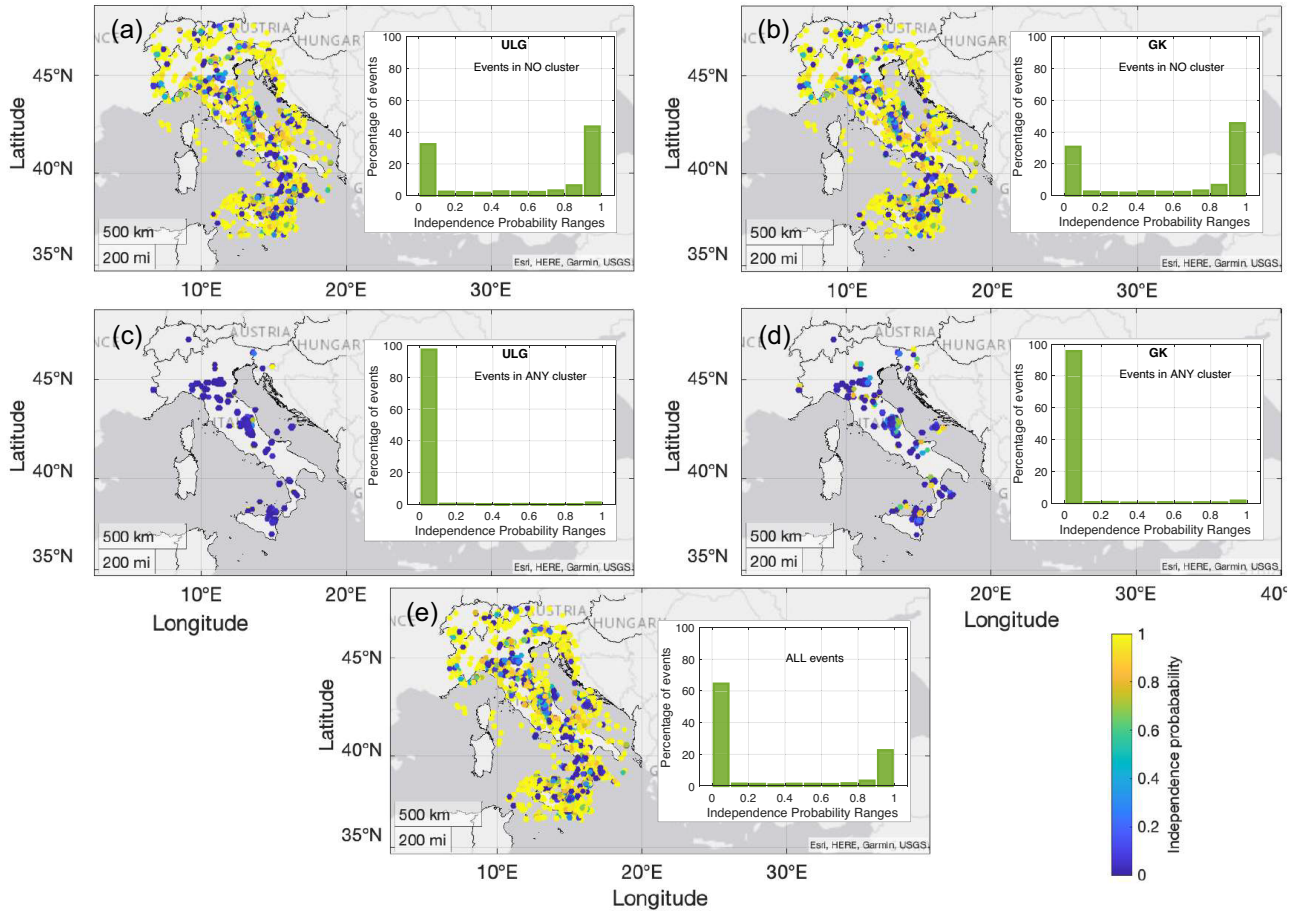

Figure 2. Seismic maps of the ISIDe events colored according to their independence ETAS probability. Top, middle and bottom panels contain the events that do not belong to any cluster, that belong to some clusters, and all the events together, respectively. The left (right) panels concern the ULG- (GK-) case. In the insets, the corresponding histograms relative to the ETAS independence probabilities associated with the events are shown.

clusters with the strongest magnitude ML 4.5+ (not smaller, for conciseness), such as the number of events and the first, last and strongest shocks. Like in the ULG-case, we count a total of 22 of these clusters, some of them do overlapping in time.

The total number of clustered events is 2653. Recalling that the cardinality of the ISIDe catalog is 5084, we deduce that there are 2431 "single" events not associated with any GK-cluster (i.e. "unclustered-GK events"). These events are either "very likely independent" or "very likely triggered", indeed 76.3 per cent of the unclustered-GK events have independence probability in the intervals $[0, 0.1]$ or $(0.9, 1]$. This can be observed by looking at panel (b) of Fig. 2, where dots are mainly yellow or dark blue, at the histogram of the relative inset, and the red dots in the top panels of Fig. 3. Panel (d) of Fig. 2, and the middle panels of Fig. 3, show instead that almost all the GK-clusterd events are "very likely triggered" (95.6 per cent). Besides the percentages, in Fig. 3 we also report the number of events considered and the sums of the expected descendants and independence ETAS probabilities. These statistics are finally summarized in Table S2 of the Supplemental Material.

4.2.3 ULG versus GK

Window-based methods (ULG and GK) agree well with the probabilities of clustered events being triggered in the ETAS model, in fact, most of the data in any cluster have independence probability < 0.1. Vice-versa, if we consider events not in clusters according to ULG and GK, the methods' response does not agree well, because $\sim 1/3$ of them still has an independence probability < 0.1. This result may suggest that the deterministic declustering methods are better at identifying triggered events than independent ones, with a high residual proportion of events being labeled independent likely to be triggered. An additional analysis on the spatiotemporal location of the unclustered-ULG and unclustered-GK events with independence probability in $[0, 0.1]$ is also discussed in the Supplemental Material (Fig. S5), where we also compare the frequency magnitude distributions of unclustered and clustered events, both in the ULG- and the GK-cases (Fig. S6, Supporting Information).

We now focus on the clusters with the strongest magnitude ML > 5.0 (hereafter, "*strongest*-ULG" and "*strongest*-GK"). We found precisely six *strongest*-ULG and seven *strongest*-GK clusters, basically containing the main sequences that occurred in Italy since 2005, like the 2009 L'Aquila sequence, the 2012 Emilia sequence and the 2016 Central Italy sequence. The complete list and relative details are reported in Appendix B. The GK procedure identifies an additional *strongest* cluster (seven instead of six) because it splits the 2012 Emilia sequence into two different clusters, each containing one of the two strongest (ML 5.8+) events that occurred (see Appendix B). This sequence is instead associated with a single cluster by the ULG procedure. Assuming that one cluster should entirely contain a single seismic sequence, as for the 2012 Emilia

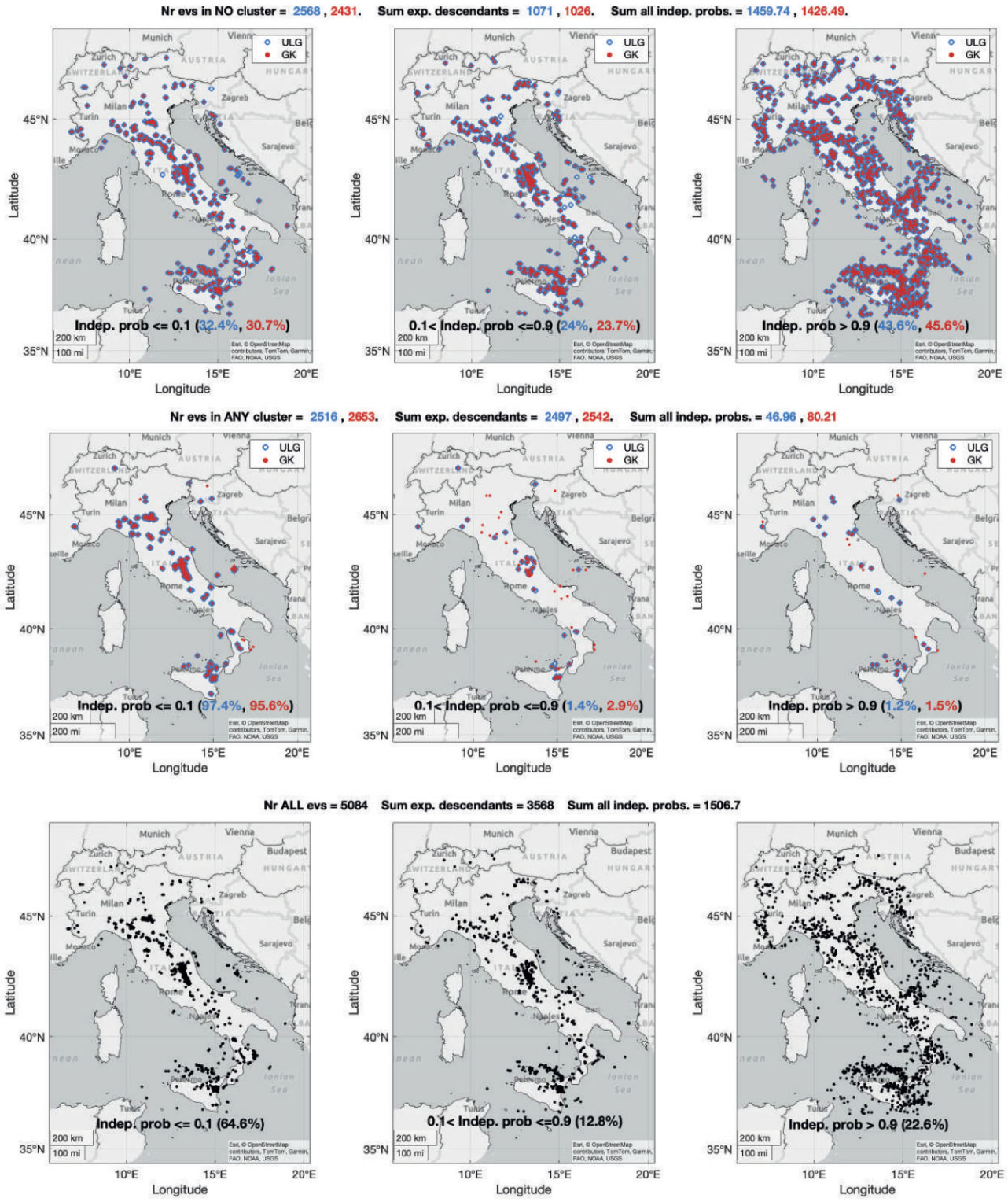

Figure 3. Seismic maps of the ISIDe events that do not belong to any cluster (top) or belong to some clusters (middle). The bottom panels refer to all the ISIDe events together. Left, middle and right panels correspond to the independence probability ≤ 0.1, in $(0.1, 0.9]$, and > 0.9, respectively (the percentage of events is also shown). Blue (red) is used for the ULG- (GK-) case. The number of events, the sum of expected descendants and the sum of all the independence probabilities are finally given for each case.

case (Scognamiglio *et al.* 2012), the GK procedure could have failed in this identification.

The spatiotemporal extensions of the *strongest*-ULG and *strongest*-GK clusters are compared in Figs 4 and 5. As regards the splitting of the Emilia 2012 sequence by GK, in the plots we considered only the longest *strongest*-GK cluster, which contains the strongest (ML 5.9) event. The maps show that the GK procedure generally associates events occurring in a slightly wider area

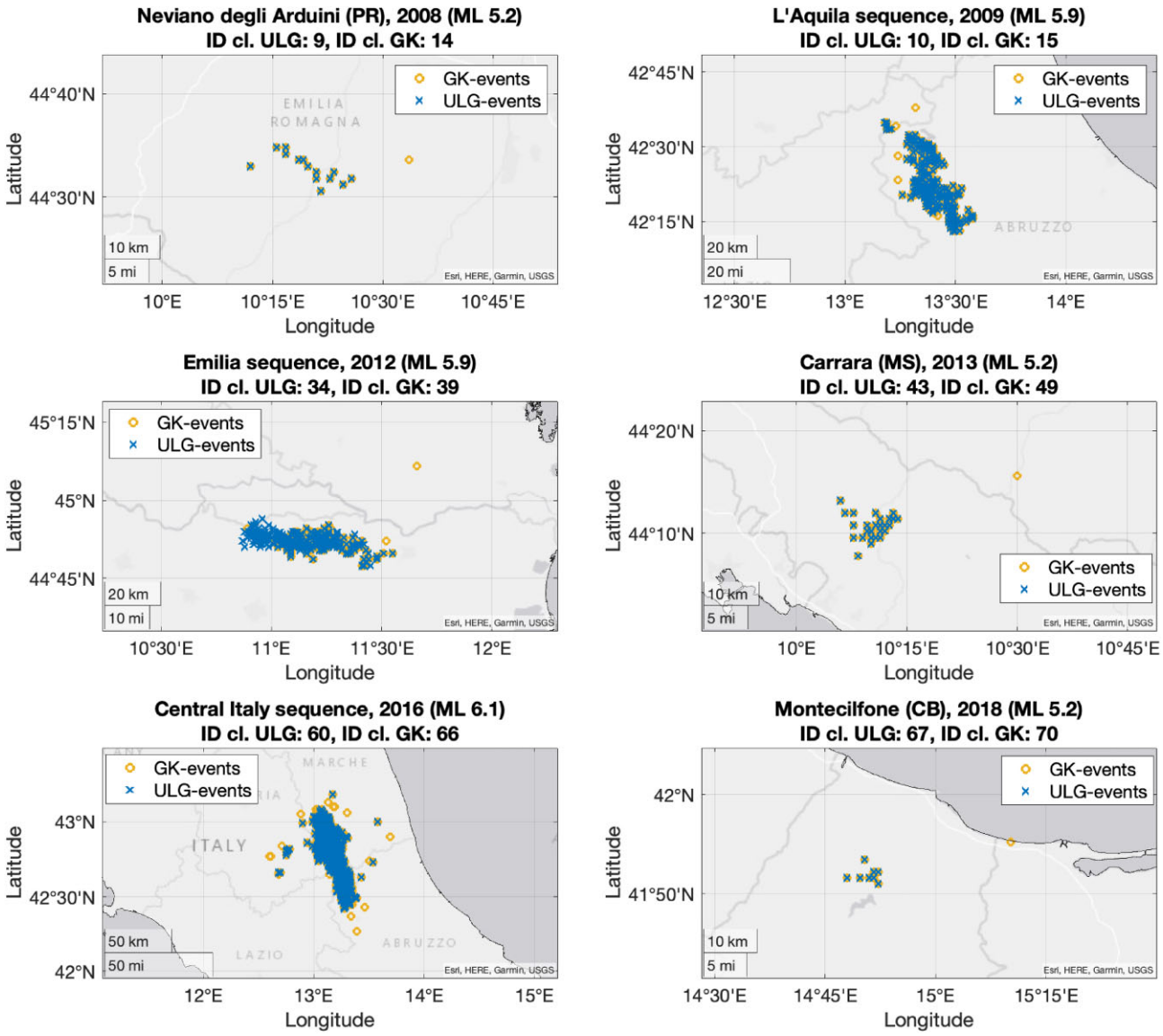

Figure 4. Seismic maps of the *strongest*-ULG and *strongest*-GK clusters (x markers and circles, respectively), that is clusters with the strongest magnitude ML > 5.0. Involved sequence, clusters ID and the magnitude of the strongest event are specified for each case.

and produces longer clusters with respect to the ULG method. On the other hand, the ULG method usually creates spatially smaller clusters, which are also shorter in time in the considered magnitude range. Compared to the alternate method, ULG may therefore fail to cluster together some aftershocks that are further away in space and time. For example, the bottom left panel in Fig. 5 shows that the ULG cluster containing the Central Italy sequence does not include the events from 2017 April on; these events are instead likely to be aftershocks of the sequence, and are indeed included in the corresponding GK cluster.

5 ASSESSING CONSISTENCY BETWEEN WINDOW-BASED IDENTIFIED CLUSTERS AND THE ETAS MODEL

The previous procedures allowed us to identify, in a deterministic way, a total of $N = 79$ ULG-clusters and $N = 82$ GK-clusters above the completeness magnitude ML 2.9, with a minimum threshold for a mainshock to generate a cluster equal to 4.0. We now aim to assess if the clustering structure is consistent with the events' ETAS stochastic measures. To do that, as explained in Section 3, we consider the events in each of the $n = 1, .., N$ clusters and, for all of them, we trace back to both: the corresponding probability of being independent, and the expected number of triggered events according to the ETAS model, computed through the approach by Console *et al.* (2010).

Let us assume that the n^{th} cluster (nCL) contains NR events. For this nCL cluster to be consistent with the ETAS model, we consider the following two simple statements.

- TEST 1: the sum S1 of the expected numbers of events triggered by the NR events in the current nCL cluster should be close to the number of elements in nCL. *Id est*, we define TEST 1 as the ratio S1/NR, and TEST 1 should be close to 1. This is because the expected offspring in the current cluster should reflect its cardinality. If we find that S1>NR, we are in the case of a productive seismic sequence spreading over a large area, likely larger than the sharp cutoffs defining the clustering domain in the window-based

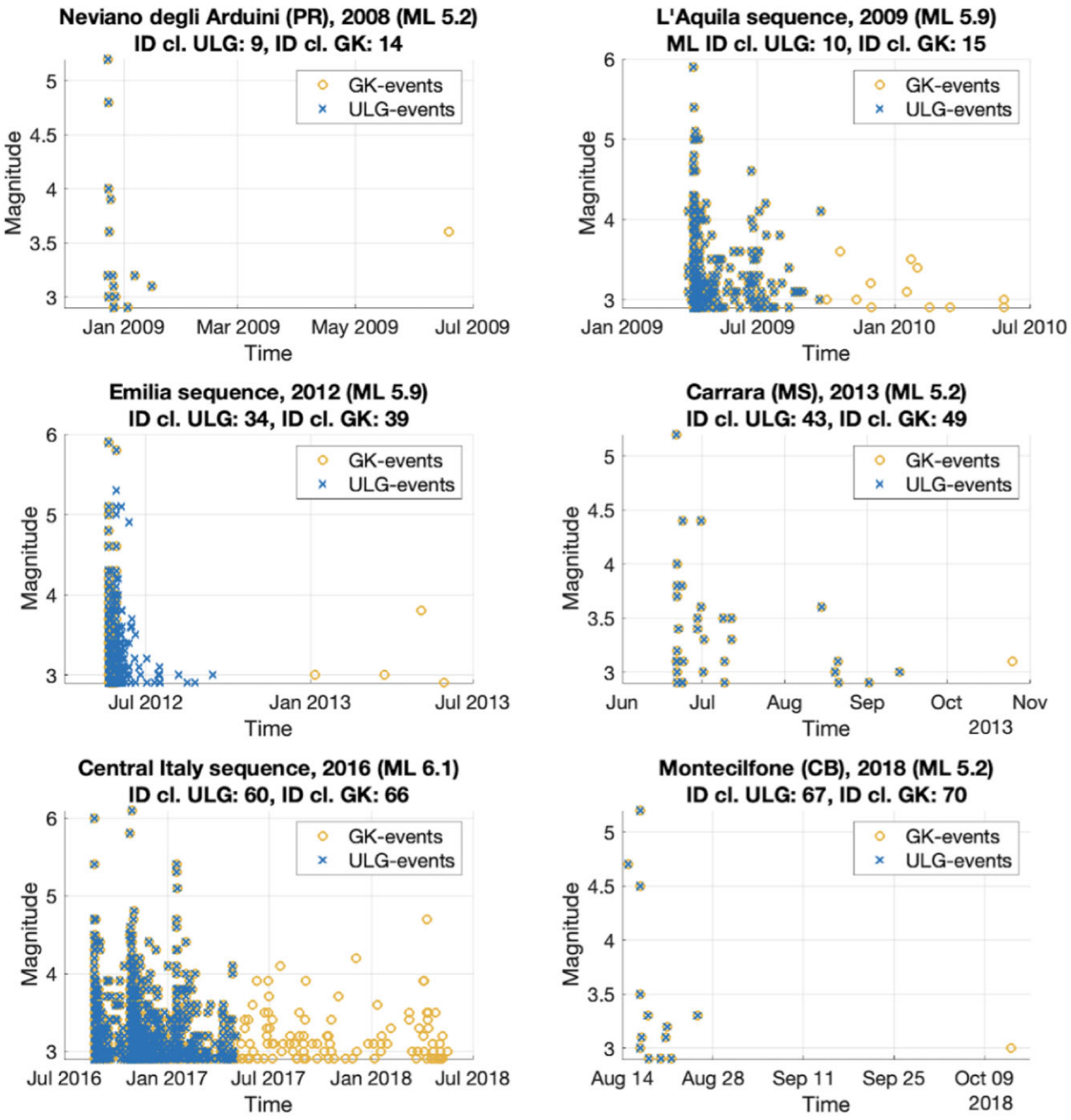

Figure 5. Magnitude VS time plot of the *strongest*-ULG and *strongest*-GK clusters (x markers and circles, respectively), that is clusters with the strongest magnitude ML > 5.0. Involved sequence, clusters ID and the magnitude of the strongest event are specified for each case.

procedure. The aftershocks of the sequence are labelled as dependent events by ETAS, but they are not all included in the cluster because of its limited domain. This could be ascribed to strong, widely spreading sequences.

- CHECK 2: The sum S2 of the independence probabilities of all the NR events in the current nCL cluster should be close to 1. *Id est*, we define CHECK 2 as |S2-1|, and CHECK 2 should be close to 0. This is because we expect a "single" cluster to have a "single" independent event. If we find that S2 > 1, we can say that the current nCL cluster has more than one independent event, and this could be the case of a complex seismic activity characterized by events which ETAS splits into different earthquake sequences (each with its own independent starting event), but that fall within the sharp cutoffs defining the clustering domain in the window-based procedure. Several ETAS-like clusters are then combined into one by the window-based clustering algorithm, thus identifying clusters containing more than one ETAS-independent event.

The first of the above statements is also statistically tested, which is why we named it "TEST 1".

In Fig. 6, we show the results of the two checks (TEST 1, x markers; CHECK 2, circles), top and bottom panels, respectively for ULG- and GK-clusters. The histograms of the test statistics are also shown in the central insets; the explicit numbers of the two checks, rounded to the second decimal, are instead summarized in

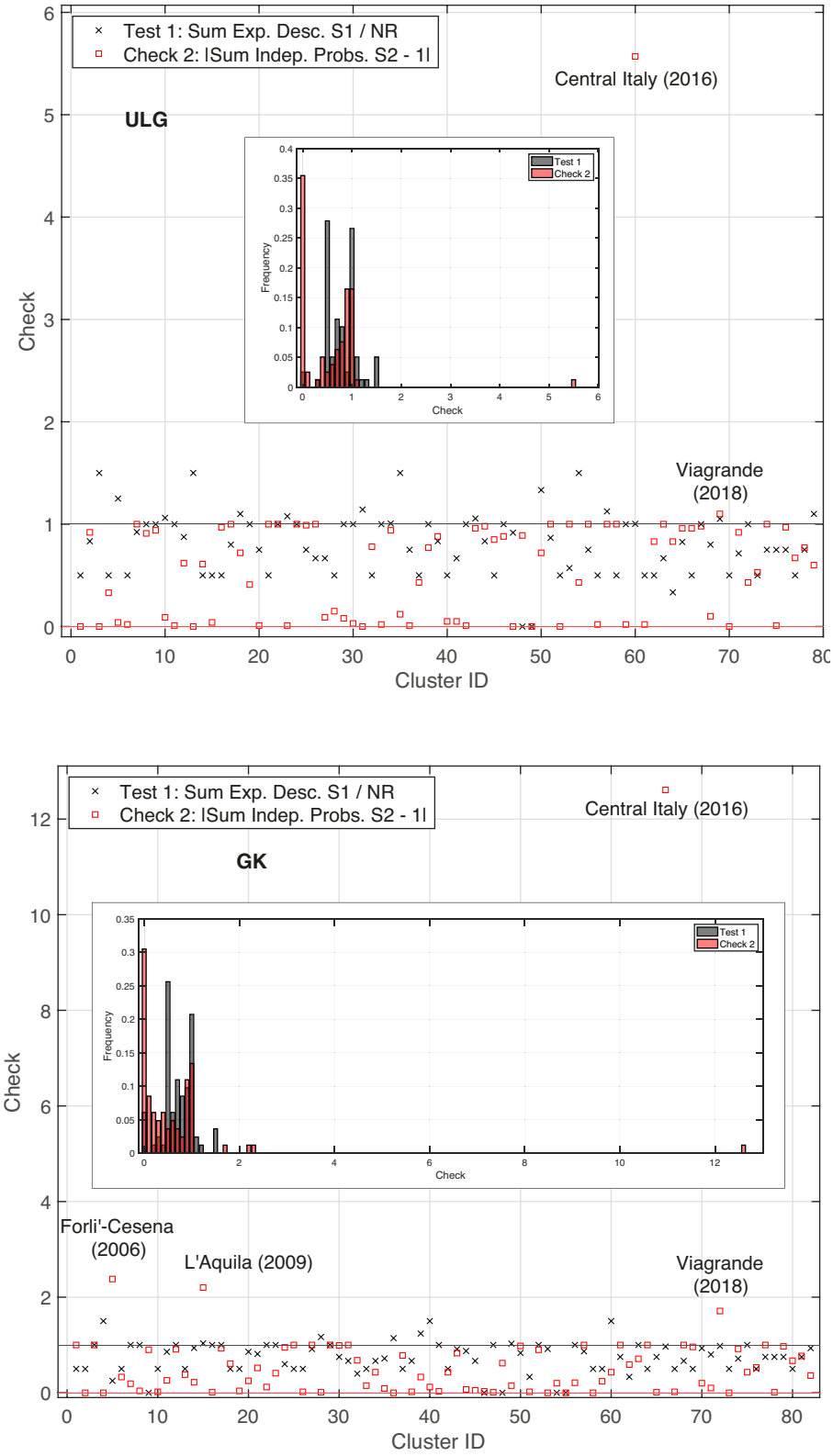

Figure 6. Graphical results of the two checks (TEST 1, x markers; CHECK 2, circles) for the ULG- and the GK-clusters in top and bottom panels, respectively. In the insets, the histograms of the test statistics.

Tables S4 and S5 of the Supplemental Material, respectively for the 22 ULG- and GK-clusters with strongest magnitude ML 4.5+ (again, not smaller for conciseness). Comparing the two panels of Fig. 6, we can see that for the majority of ULG-clusters TEST 1 ranges between 0.5 and 1.5 (Mean = 0.805, Median = 0.8, Standard deviation (Std) = 0.308); in the GK-case, we observe instead a

slightly higher number of clusters for which TEST 1 ≤ 1, precisely ranging between 0.5 and 1 (Mean = 0.737, Median = 0.75, Std = 0.324). This shows that the GK algorithm tends to systematically slightly overestimate the number of events in the clusters expected by ETAS, more than the ULG procedure does.

For both ULG and GK, the largest number of clusters has CHECK 2 close to 1 (ULG: Mean = 0.596, Median = 0.67, Std = 0.708; GK: Mean = 0.647, Median = 0.395, Std = 1.427). Except for a very few outliers for which CHECK2 > 1, in the remaining cases CHECK 2 is distributed between 0 and 1: a clearer pick around this latter value is observed in the ULG case than in the GK one, which instead shows a more uniform distribution. A slightly higher number of GK-clusters proven consistent with ETAS according to CHECK 2 is then inferred.

In what follows, we will present and discuss more detailed results of the two consistency checks. For clarity, we will also graph the clusters with the strongest magnitude ML > 5.0 (*strongest*), and all the others, separately.

6 CONSISTENCY RESULTS

6.1 TEST 1

The number of events NR in each cluster versus the corresponding sum S1 of expected descendants are given in Fig. 7, respectively panels (a) and (b) for ULG- and GK-clusters. In both panels, the *strongest* clusters (i.e. those with the strongest magnitude > 5.0) are represented in the top-right thick orange axes, whereas the other clusters are given in the bottom-left thin black axes. The largest differences in absolute value between the two numbers NR and S1 are obtained for two strong earthquake sequences: L'Aquila 2009 and the Central Italy 2016 (see Appendix B for these senquences' details). These represent the strongest sequences experienced in Italy in the last decades, and the discrepancy observed between NR and S1 is mainly due to the strong temporary incompleteness they entailed into the catalogue.

Although smaller, a difference is obtained also for the ULG-cluster with ID 65, which contains the moderate Muccia sequence that occurred in 2018 April (Macerata province, Marche region; strongest event on 2018 April 10 with ML 4.7, M_w 4.6). This sequence is related to the Central Italy one, which indeed was characterized by a strong seismic activity that extended for several years. The Muccia sequence (2018) is in fact included in the GK-cluster containing the Central Italy sequence, for which the largest discrepancy between NR and S1 is observed.

A quite significant difference is also observed for the two GK-clusters containing the two strongest events (ML 5.9 and ML 5.3) of the Emilia sequence 2012 (see Appendix B). We recall that the GK procedure associates these events to separate clusters.

Overall, although the short-term aftershock incompleteness clearly plays a relevant role in TEST 1, the comparison between NR and S1 suggests that the number of triggered events, expected by the ETAS model, well reflects the clustering structure deterministically identified.

In fact, the consistency of both the ULG- and GK-clusters with ETAS as regards TEST 1 is statistically significant: a correlation test returned that S1 is highly positively correlated with NR (p-value = 1.76e − 140 and 1.87e − 107 for ULG- and GK-cases, respectively), and the linear fit of the points (S1, NR) has slope 1. Results are shown in the top panels of Fig. 8 (ULG- and GK-cases in left and right columns, respectively), where the linear fit is very close to the bisector. Residuals are given in the bottom panels of the same figure. The correlation results are also not sensitive to the high-leverage points (Rousseeuw & Van Zomeren 1990), that is, clusters whose number of events is far away from the other cases, like for example the ones with the Central Italy 2016 sequence. This is demonstrated in detail in Section S1 of the Supplemental Material.

6.2 CHECK 2

In the majority of both ULG- and GK-clusters, CHECK 2 ranges between 0 and 1, as shown in Fig. 9, panels (a) and (b), respectively for the *strongest* clusters and the others, and red/blue for GK-/ULG-cases. Mean, Median and Std of S2 in the case of ULG-clusters are 0.594, 0.4 and 0.833, respectively. The same quantities for the GK-clusters are instead 0.978, 0.833 and 1.568: this latter value outlines a variable behaviour from one GK-cluster to the other. Interestingly, the GK-clusters with S2 much larger than 1 are more in number than in the ULG case; for example, the GK-clusters with S2 > 1.2 are 13 more than in the case of ULG. This is related to the fact that GK-clusters are usually larger and longer than ULG. Therefore, they typically contain a higher number of events, thus resulting in a higher value of the sum S2 of the events' independence probabilities.

By looking at panels (a) and (b) of Fig. 9, we also observe two clusters, common to the two procedures ULG and GK, for which the quantity S2 is notably larger than 1 (see also the red squares in Fig. 6). The first contains the Central Italy sequence, and this is certainly due to the high productivity of the sequence itself. The second cluster contains instead the moderate Viagrande sequence (Catania province, Sicilia region) that occurred in 2018 December, with the strongest event on 2018-12-26 with ML 4.8 (M_w 4.9). The proximity of this sequence to the Etna volcano allows us to ascribe it to a seismic activity of volcanic type, which is known to be driven by mechanisms not well captured by the ETAS model.

Regarding only the GK case, two additional clusters are not well inferred by S2. These are the one with L'Aquila sequence 2009 (we infer this is due again to the high productivity), and the cluster containing a small sequence occurring between the provinces of Forlí-Cesena (Emilia-Romagna region) and Arezzo (Toscana region) in the spring of 2006, with the strongest event on 2006 April 16 having magnitude ML 4.1 (M_w 4.3). Since this sequence was neither not so highly productive, nor characterized by very strong events (about five events with ML 3+ and one event with ML 4+ within a radius of 50 km from the strongest one, in the period 2006 April–August), further investigations are needed to explain this result.

The histograms given in panels (c) and (d) of Fig. 9, respectively for ULG- and GK cases, show that the highest frequencies of S2 are observed around 0 and 1. In the ULG-case, we precisely find a total of 53 (out of 79) clusters with S2 < 0.1 or $0.9 <$ S2 ≤ 1.1, while for the GK-case this total is 41 (out of 82). Recalling that CHECK 2 is satisfied when S2$\sim$1 (see Section 5), the high bars around 1 imply consistency between the corresponding deterministically identified clusters and their events' ETAS independence probability. However, these panels also show a high bar around 0, suggesting that the clusters in this group are inconsistent with ETAS. This result may be a consequence of excluding foreshocks in the clustering identification procedure (see Section 4.1). A further discussion will be given in Section 6.2.2 below.

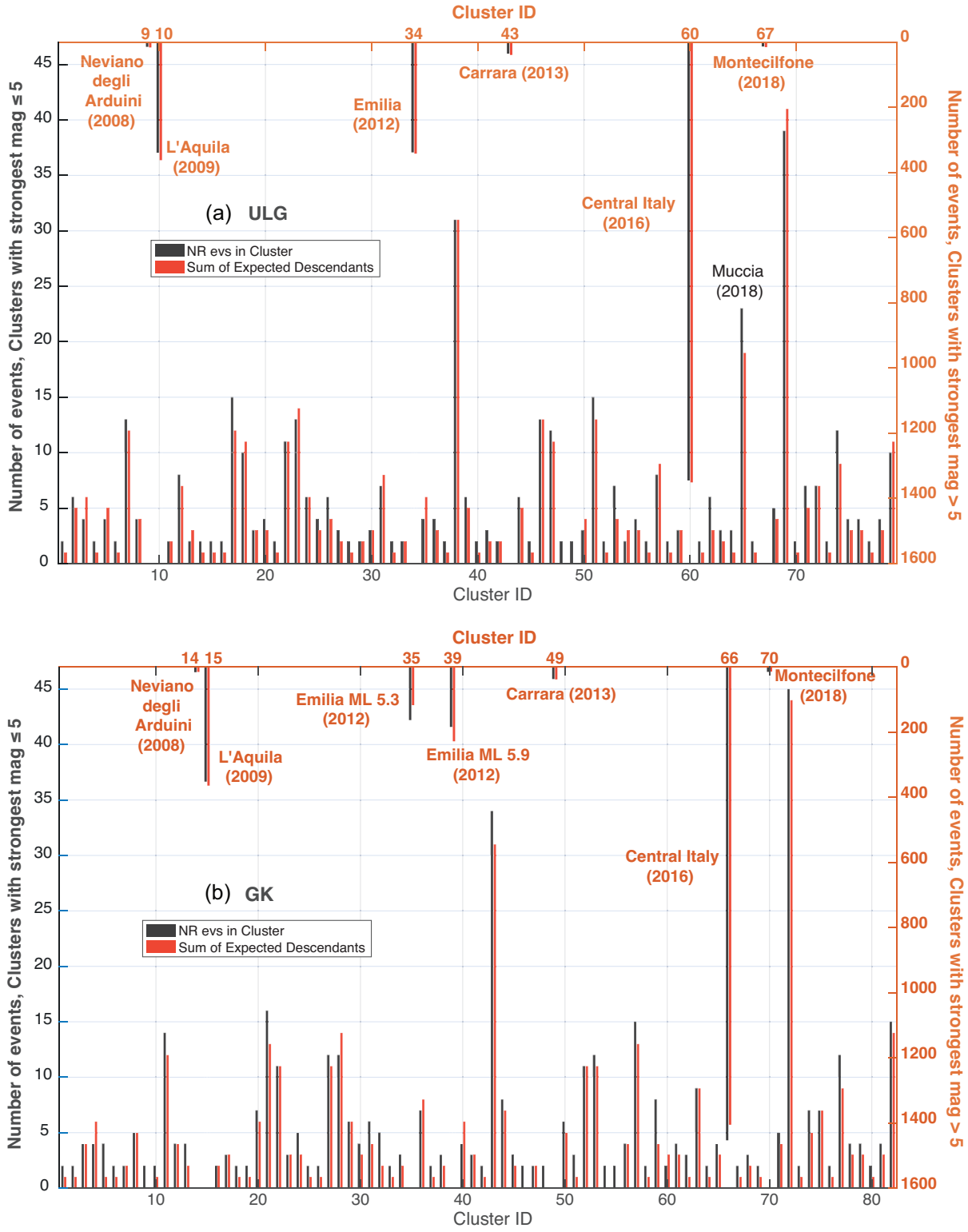

Figure 7. Histograms relative to the number of events and the sum S1 for each cluster, panels (a) and (b), respectively for the ULG- and the GK-case. In each panel, bottom-left thin black (top-right thick orange) axes concern the clusters with the strongest event having ML $\leq$ 5.0 (ML $>$ 5.0).

The bimodal behaviour of S2 shown in the histograms of panels (c) and (d) of Fig. 9, that is, the high frequencies around both 0 and 1, clearly invalidate any possible statistical test in favour of S2 being distributed as a random variable with mean 1, a condition that would statistically validate CHECK 2 (see Section 5). In the next section, we then examine more in detail the results obtained for S2, to search for a possible correlation between its distribution, and the distribution of some clusters' characteristics.

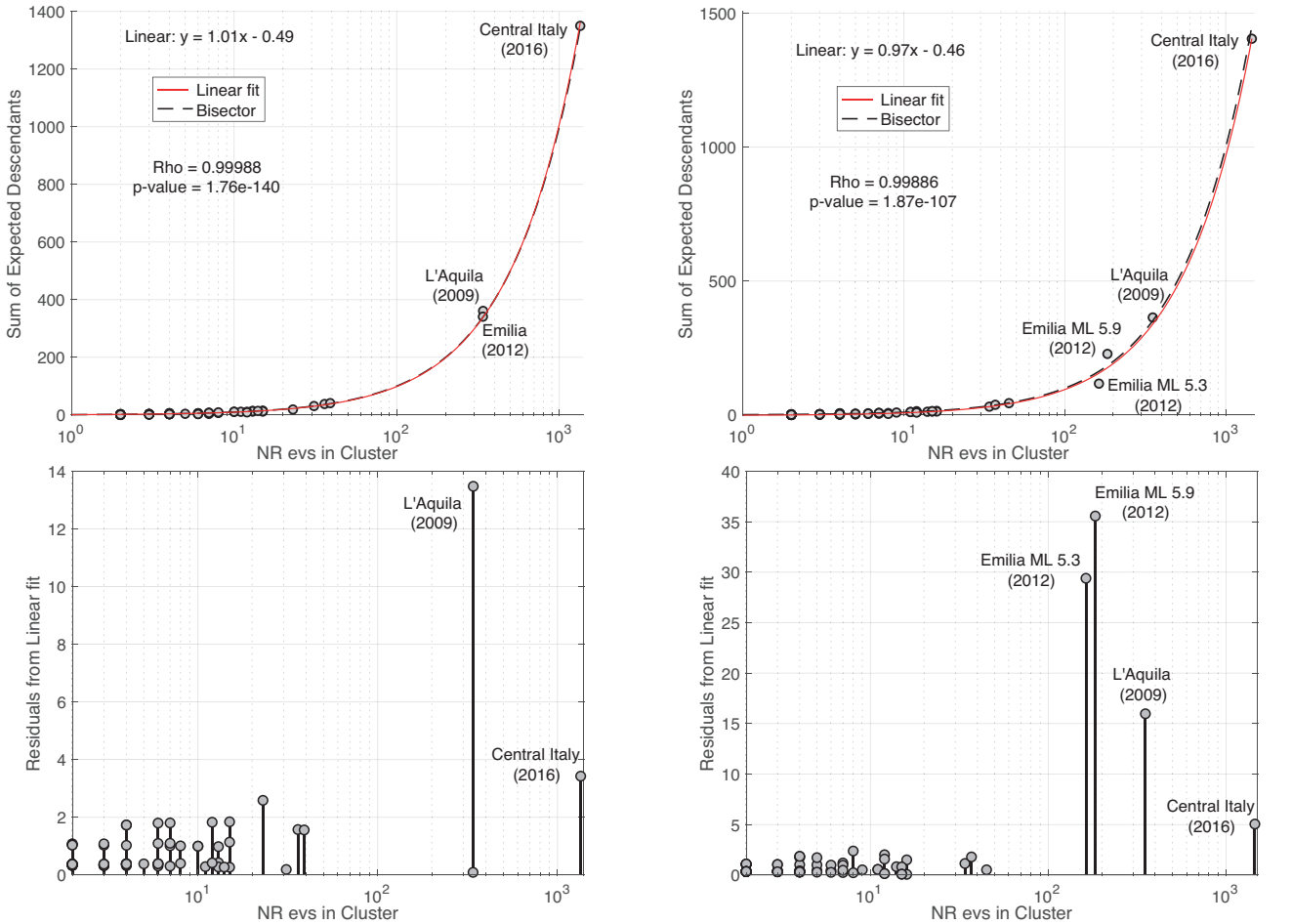

Figure 8. Correlation analysis between the sum S1 of expected descendants and the number of events in the cluster, in support of TEST 1 results, relative to the ULG- and GK-clusters in left and right panels, respectively, in logarithmic x-scale. Top panels show the linear fit of the data (dashed line, equation line written in top left), the comparison with the bisector (continuous line) and the correlation test results. Bottom panels show instead the residuals of the data with respect to the linear fit.

6.2.1 In-depth analysis of S2 distribution

One of the main quantities that are worth investigating to search for a possible pattern driving the S2 distribution is surely the magnitude. In particular, the distribution of the magnitude of the clusters' mainshocks, combined with the number of events, may correlate the quantity S2 with the size of the seismic sequence involved in the cluster. The maximum magnitude is also related to the type of zone (compressional and extensional) where the cluster occurs. In Fig. 10, we plot the independence probability S2 versus the number of events in each cluster and the clusters' mainshocks' magnitude, for the ULG- and the GK-cases in panels (a) and (b), respectively. Just for a more straightforward graphical interpretation of the figure, two clusters with >400 events (one ULG and one GK) are not represented; otherwise, all the other points in the scatter plot would have appeared crowded around the minima of *x*- and *y*-axes. No clear correlation is observed between the three considered variables, except for a very slight tendency of clusters with a high cardinality to have a smaller S2. Besides, the higher the mainshocks' magnitude, the clearer it is that the great majority of S2 values are either very close to 0, or very close to 1.

To verify the existence of a spatial pattern, we mapped the clusters with S2 approaching these two values. Specifically, clusters with S2 > 0.9 and S2 < 0.1 are given in Fig. 10, panels (c) and (d) for ULG- and GK-cases, respectively. In both the maps, a high density of S2 larger than 0.9 can be observed in the Central Apennines, while S2 < 0.1 stands out in the Northern part of this Mountain Chain. Interestingly, an opposite S2 behaviour is observed in the Emiliana Po valley for ULG- and GK-clusters, the latter showing S2 > 0.9, the former S2 < 0.1. The higher ETAS independence probability of the events involved in the GK case, actually agrees with the fact that, differently from ULG, the GK procedure splits the two strongest events of the 2012 Emilia sequence into separate clusters, thus resulting in more than one mainshock. Further analyses are required to better investigate any possible correlation between the S2 values and a physical characteristic of the seismic process, to be framed also from a statistical point of view. This will be the object of future studies.

6.2.2 CHECK 2 inconsistency cases: S2 $\sim$ 0 or S2 $\gg$ 1

The results illustrated in Section 6.2 have shown that some ULG- and the GK-clusters are inconsistent with the ETAS independence probability. In fact, in some cases, the sum S2 of clusterized events' probability of being independent is not close to 1, as required in CHECK 2.

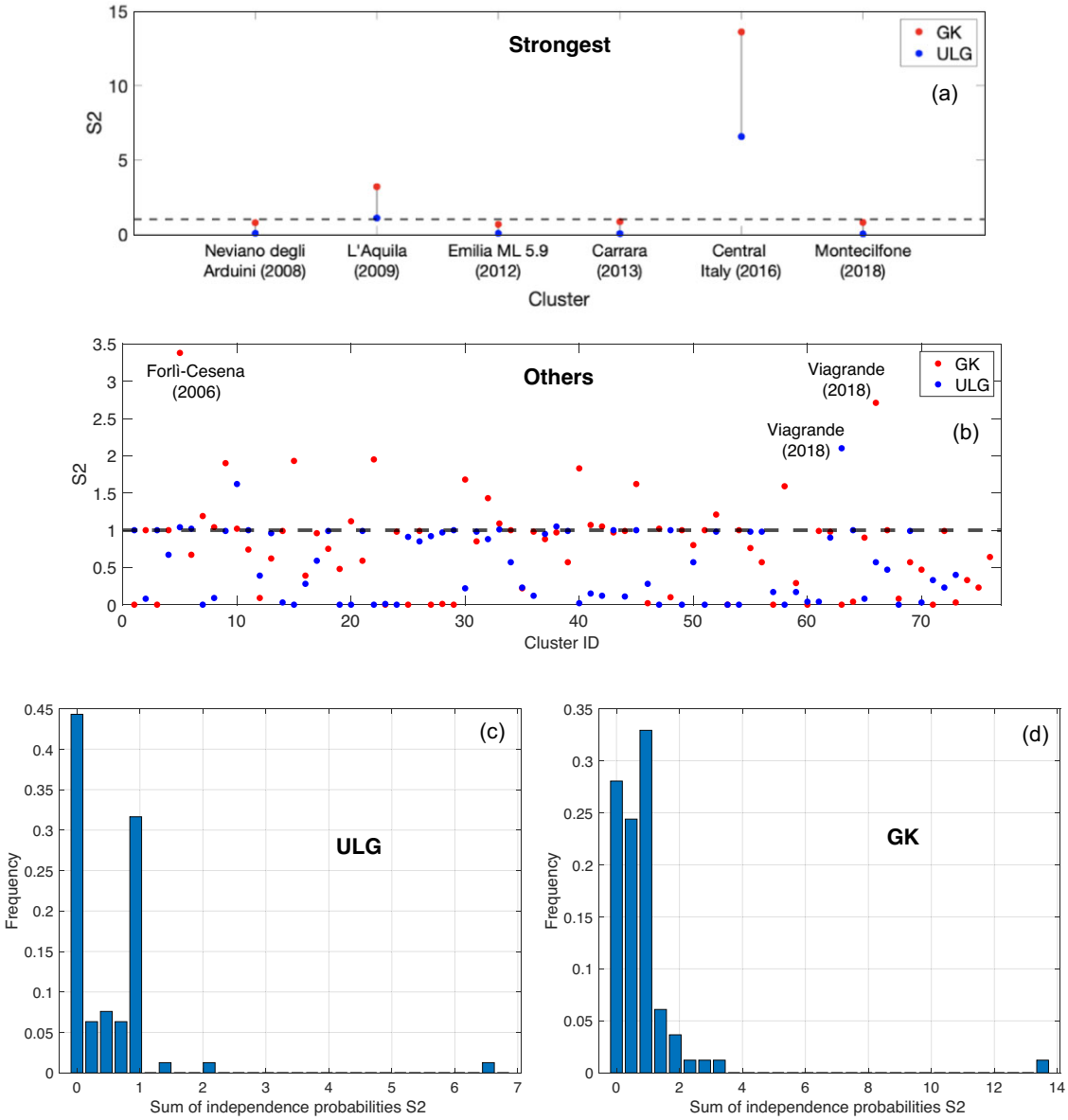

Figure 9. Panels (a) and (b), respectively for the *strongest* clusters and all the others, show the comparison between the sums S2 of the independence probabilities relative to GK-clusters (red points) and ULG-clusters (blue points). Panels (c) and (d) show instead the histograms of the sum of independence probabilities S2, respectively for ULG- and GK-clusters.

The largest number of inconsistency cases consists of clusters not containing any event labelled as "very likely independent" according to ETAS, that is all the clusterized events are triggered, and consequently S2 is close to 0. As anticipated in Section 6.2, a reason for that could be the exclusion of foreshocks in the clustering identification procedure, in order to avoid creating multiple assignments. It therefore could happen that a strong earthquake, considered as a foreshock, generates the events included in a cluster, but is identified by the clustering algorithm as an independent event because of how we setup the method. Consequently, the included events have low-ETAS independence probabilities, and the relative sum S2 approaches 0.

Another situation that could lead to S2 $\sim$ 0 is when a strong mainshock is followed by a strong aftershock, and the identification procedure splits these events, and the other aftershocks, into different clusters. Because multiple assignments are prevented, the mainshock is included in just one of the possible clusters of aftershocks. At the same time, the entire sequence could spread just beyond the sharp cutoffs imposed by the window-based methods. Sharpness is generally bound to cause a problem due to the distances in space and time being mixed (Bayliss *et al.* 2019).

Although fewer, some ULG- and GK-clusters are proven inconsistent with respect to CHECK 2 not because S2 $\sim$ 0 but, on the contrary, because the sum S2 of their events' independence probability is much higher than one. This implies that they contain more than one "very likely independent" event, that is a mainshock in the ETAS setting. At first glance, a high value of S2 ($\gg$1) could be thought of as the effect of a particularly high number of triggered events, higher than those expected by the Omori law for a

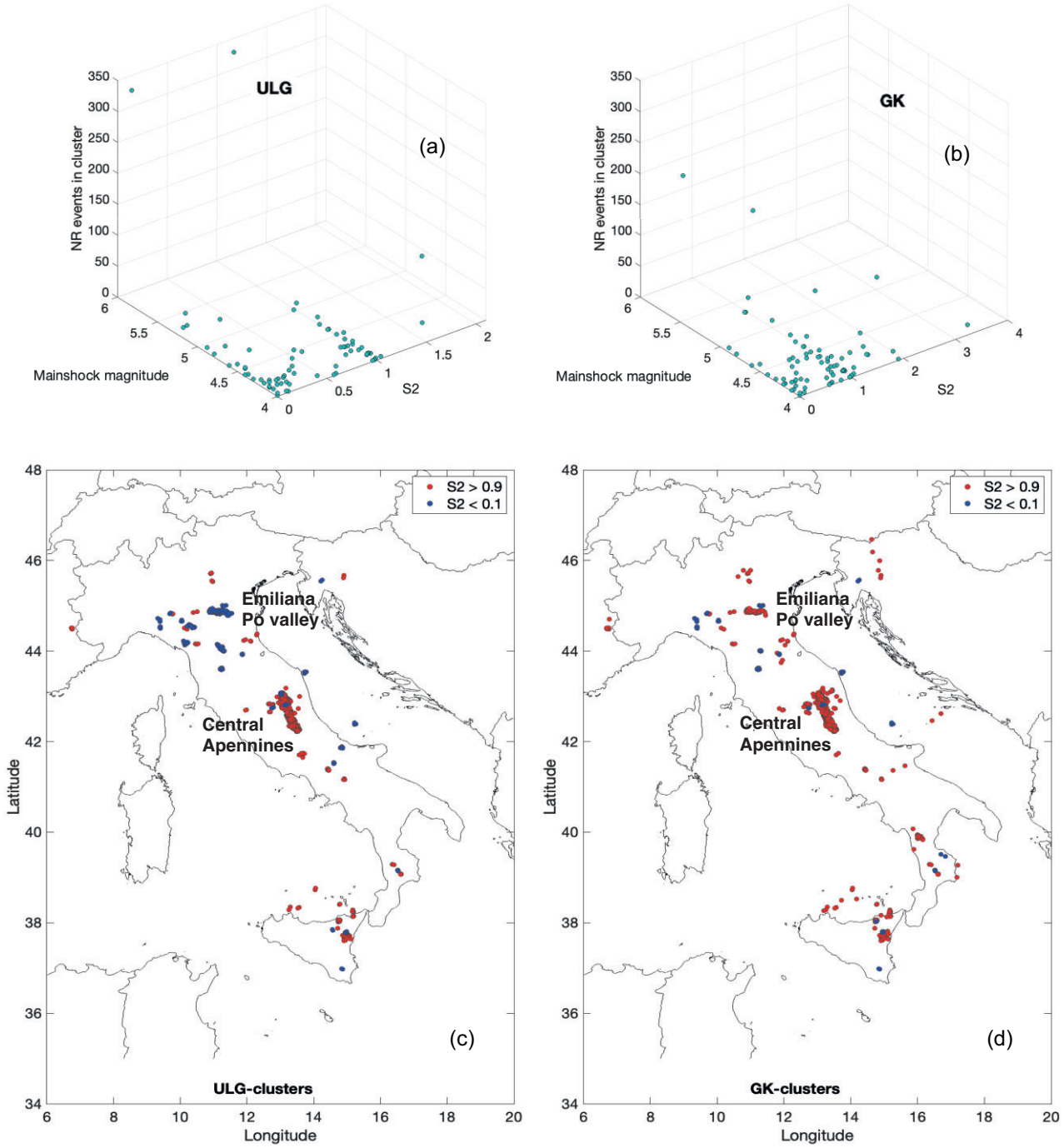

Figure 10. Panels (a) and (b) show the 3-D scatter plots of the number of events in each cluster versus the independence probability S2 (x-axis) and the clusters' mainshocks' magnitude (y-axis), respectively, for the ULG- and the GK-cases. To prevent points from being crowded around the minima of x- and y-axes, two clusters with >400 events (one ULG and one GK) are excluded. Panels (c) and (d) show instead seismic maps of clusters' events with S2 $>$ 0.9 (red points) and S2 $<$ 0.1 (blue points), respectively for ULG- and GK-cases.

single sequence (Spassiani & Marzocchi 2018). However, an in-depth analysis showed that, in our case, the real influence on S2 is given by the events with high-independence probability, even if they are a few and no matter how numerous the aftershocks are. An example is given in Fig. 11, where we plot the cumulative independence probability of the GK-cluster containing the Central Italy sequence. The first event in this cluster has an independence probability close to 1, implying that it is a "real mainshock". After a series of events with low independence probability, including the strong shocks of 2016 October and November, the sequence starts its second phase of epicentres' spatiotemporal scattering, characterized by events with high-independence probability, reaching its maximum on 2018 May. More than 50 per cent of S2 consists of the ten strongest events, thus confirming that, in our case, a cluster with CHECK 2 larger than 1 contains more than a "very likely independent" event. Besides, the clusterized events' independence

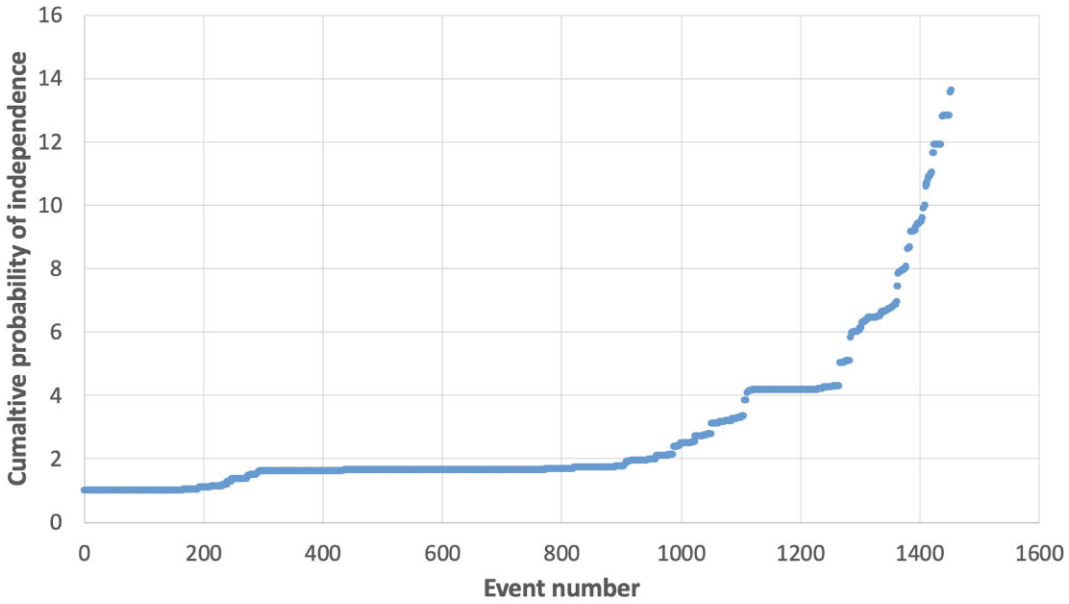

Figure 11. Cumulative ETAS probability of independence for the GK-cluster containing the Central Italy sequence (2016).

probability increases with their spatiotemporal distance. The cumulative independence probability for the other *strongest* clusters, both for GK and ULG cases, is given in Fig. S7 of the Supplemental Material.

6.3 Focus on two interesting clusters

An interesting focus can be on two clusters involving two sequences of interest for the Italian territory. The first one started with the Montecilfone event (Campobasso province, Molise region), which occurred on 2018 August 16 with ML 5.2 (M_w 5.1). This sequence actually belongs to one of the *strongest* clusters (see Appendix B) introduced in Subsection 4.2.3, and was characterized by some peculiar statistics, such as the number of aftershocks that was lower than expected from the classical decreasing power Omori law adopted in statistical seismology (Moretti *et al.* 2018). The ULG- and GK-clusters including the Montecilfone sequence (respectively with ID 67 and ID 70) contain a few events: 14 and 15, respectively. They are precisely the same events, except for the last one in GK, which gets this cluster a bit longer and wider than ULG (see also bottom right panels of Figs 4 and 5). Because of this single event, the GK cluster lasts about two months instead of the ∼10 d of the ULG case. Interestingly, this event has no expected aftershocks according to ETAS. Consequently, the sum S1 of expected descendants is the same in the two cases and, since it is computed equal to 14, the ratio S1/NR for TEST 1 turns out to be precisely 1 for the ULG cluster, and ∼1 for the GK one. This highlights that the number of expected aftershocks reflects well the cardinality of the cluster, therefore consistency is proven in this case.

As regards the second check, the single additional event belonging to GK has a 77 per cent probability of being independent. In Section 6.2.2, we have shown that the sum S2 of independence probability is influenced almost only by the events with a high-independence probability, and this is indeed confirmed in the Montecilfone sequence, for which we find S2 = 0.02 in the ULG case and 0.8 in the GK one. The consistency with ETAS in terms of CHECK 2 is then not satisfied regarding GK, whereas, for ULG, it still needs to be completely convincing because S2 is higher than before but still lower than 1. The ETAS independence probability for the last event in GK is indeed not definitely high (e.g. > 0.9). This may suggest that the Montecilfone sequence was not characterized by a "true mainshock" according to ETAS. The reason could be related to a previous 4.2 event, which struck the same region four months before, followed by a very low-magnitude sequence. This is the topic of another paper, based on enhanced earthquake catalogues (Gentili *et al.* 2024).

The second cluster that is worth focusing on, is the one containing the Pollino sequence (Cosenza province, Calabria region), which occurred in 2012 September–October with the strongest earthquake on 2012-10-25 having magnitude ML 5.0 (M_w 5.2) – (ULG cluster ID 38 and GK cluster ID 43). This sequence was characterized by a very productive seismic activity of moderate-to-low size. The cardinality of the ULG- and GK-clusters involved is in fact about double that of the previous case. The ULG-cluster contains 31 events; these same events and three additional ones are instead in the GK-cluster, these latter three events making again the GK cluster a quite longer and wider cluster than ULG (the map is given in Fig. S8 of the Supplemental Material). The temporal extent is about 2 and 5 months, respectively, in the ULG and GK-cases. The three additional events in GK have respectively 0.68, 0.004 and 0.91 probability of being independent, and 0, 0.11 and 0.006 expected number of descendants according to ETAS. The ratios S1/NR for the ULG- and GK clusters involved are then similar, because so are the sums of expected descendants and the cardinalities. Precisely, we found S1/NR=1 and 0.91, respectively, thus proving consistency concerning TEST 1 for both ULG and GK.

As regards CHECK 2, we instead find a different situation. The ULG- and GK- clusters containing the Pollino sequence have S2 = 0.23 and 1.83, respectively. Two of the three additional events have a high-ETAS independence probability, one of which definitely high (=0.91). Since the ULG-cluster does not contain these two likely independent events, and all the others are very likely aftershocks, according to ETAS it does not contain a "true mainshock" of the considered sequence. The event with independence probability of

0.91 is even unclustered by the ULG procedure. CHECK 2 is therefore not satisfied in this case. The same holds true for the GK-cluster, but inconsistency has now been proven because of the opposite situation. Again, two of the three additional events in GK are likely independent and, even if one is more likely independent than the other, they both play a relevant role in S2, which indeed is closer to 2 than to 1. According to ETAS, the GK cluster contains then two events that may have generated the Pollino sequence.

A window-based, probabilistically consistent cluster could have been the ULG one that also included the event with very high-independence probability. This example shows again that the deterministic methods better identify dependent events than independent ones. In the case of certain complex seismic sequences, we cannot apply the deterministic techniques, which inevitably lose much information about the sequence itself. Instead, it could be recommendable to relax the framed concept of window-based clusters, resorting to the purely probabilistic approach that better stands to reason when describing the behaviour of these complex earthquake sequences.

7 CONCLUSIONS

In this paper, we used a (probabilistic) ETAS-based approach to make inferences about the clustering structures obtained through the deterministic, window-based method. The catalog used in our analysis is the Italian ISIDe catalog from 2005 April 18 to 2021 April 30. In order to check for consistency between the deterministic and the probabilistic approaches, we first identify clusters by applying two window-based clustering procedures: Gardner–Knopoff (GK) and Uhrammer–Lolli–Gasperini (ULG). Then, independently of the clustering structures identified, we associate with all the events in the catalog both the probability of being independent and the expected number of aftershocks derived from the ETAS model. Finally, we develop an automatic approach based on two simple checks (TEST 1 and CHECK 2) to assess whether the ETAS stochastic measures associated with the clustered events coherently reflect the identified clustering structures.

It is important to stress that the methodologies adopted here are completely unaware of any underlying physical process. In fact, on the one hand the ETAS model just assigns a probability to the events being triggered or independent according to a purely data-driven stochastic process; on the other hand the window-based approach simply gathers events that are close in space and time. They unconsciously consider any type of interaction (stress transfer, fluid migration, aseismic creep, ecc.) as a possible cause for earthquake clustering, as long as events occur in limited spatiotemporal windows. A future development may include the physics behind the seismic process for example in the parameters' physical modelling.

Our analysis has shown that no substantial difference is observed in the application of the two window-based procedures by ULG and GK. The cardinality and mainshocks of the corresponding identified clusters are comparable (see for example Tables S1 and S3 of the Supplemental Material, which concern the clusters with the strongest magnitude ML $\geq$ 4.5). The only discrepancy can be appreciated in the fact that GK identifies quite longer and wider clusters when considering strong mainshocks than ULG, and this is a direct consequence of the specific different set of equations used to determine clusters' extension (explicit formulas in Appendix A; graphical representation in Fig. S2 of the Supplemental Material).

Results concerning the comparison between the deterministic and the probabilistic approaches have proven an overall consistency in terms of the number of expected descendants (TEST 1). Indeed, the sum S1 of aftershocks expected by the ETAS model for the events in any cluster well reflects the cardinality NR of the cluster itself. S1 is significantly positively correlated to NR, the pairs (S1, NR) being also fitted by a linear model with slope 1.

The second check we applied showed less clear results. In this case, consistency was proven when the sum S2 of the events' independence probabilities within a cluster is close to 1, implying the presence of a single "very likely independent" event (e.g. mainshock). Both for ULG and GK procedures, we find S2 close to 1 for several clusters, but there are also several other cases for which S2 $\sim$ 0 or S2 $>$ 1. These inconsistencies may be related to excluding foreshocks in the clustering identification procedure so as not to create multiple assignments. It therefore may happen that a strong earthquake, labelled as foreshock and with a high-independent ETAS probability, generates events in a cluster to which it is not assigned. Another situation that could lead to inconsistency in terms of S2 is that of a complex seismic activity characterized by events which ETAS splits into different earthquake sequences, each generated by a different mainshock, but falling within the sharp cutoffs defining the clusters' extent in the window-based procedure, thus resulting in S2 $>$ 1.

We have shown that the independence probability tends to increase in the final part of a sequence (higher spatiotemporal distances between events) and that early aftershocks do not significantly contribute to S2, regardless of how many there are. This is also consistent with the smaller values of CHECK 2 obtained for the ULG approach than for the GK one, this latter generally constructing quite longer and wider clusters. The identified clusters' response to CHECK 2, and precisely the fact that ETAS recognizes more than a single independent event in some clusters (S2 $>$ 1), may reflect also that the window-based identification procedures require the labelling of an event as a mainshock to be performed, while ETAS does not account for such labelling. A slight tendency of the spatial pattern is finally obtained for clusters with S2 $>$ 0.9, which more densely occur in the Central Apennines.

The results we obtained are not biased by the specific choice of $M_m = 4.0$ as the minimum magnitude for a mainshock in a cluster. In fact, we repeated all the analyses performed in this paper by setting $M_{\mathrm{m}} = 2.9$, that is, equal to the completeness threshold. For conciseness, these results are not included here, but they show no substantial difference with those illustrated above, and the conclusions to be drawn remain the same.

Taking stock, we can state that although the application of the two window-based clustering procedures is somewhat subjective due to the subjectivity of the equations adopted, the inconsistencies inferred between deterministic and probabilistic approaches are mainly associated with the overlapping populations of dependent and independent events in the stochastic declustering procedure. Deterministic methods are found better at identifying dependent events than independent ones, with a significant number of events identified as being independent, having a high probability of being triggered in the ETAS model. On the other hand, the window-based method imposes a sharp cutoff to include events or not in a cluster, therefore this method could never entirely capture the stochastic measures associated with the events by the ETAS declustering algorithm.

A relevant point to stress is that sequences with a single "mainshock" are not always easily discernible from sequences contain-

ing many of small-to-moderate events (swarms). Such distinction is generally better captured by a probabilistic approach such as ETAS. Similarly, a strong event following an earlier strong one can be associated with this latter's same cluster, or to a different cluster, depending on the cluster identification method adopted and the specific magnitudes considered (an example here is the Emilia sequence). Instead, aside from that, the ETAS model would associate with both these events a specific probability of being independent. In general, the probabilistic approach better stands to reason in the case of certain complex seismic sequences, for which much information is lost when adopting a deterministic procedure.

To conclude, deterministic and probabilistic approaches allow us to pursue the analysis from two different perspectives, and highlight different aspects of seismicity. Except for selecting the stochastic model to consider, the purely probabilistic view is less subjective because it does not account for a specific threshold to characterize events, for example, being in a cluster or not. Still, the concept of probability is challenging to understand and interpret, and of course, by definition, it carries a certain degree of uncertainty.

Object of a work in preparation (for reference, see Tavani & Spassiani 2023) is the analysis of network properties of seismic clusters based on a third approach, less parameter-dependent, that is the NN by Zaliapin *et al.* (2008) and Zaliapin & Ben-Zion (2013) (see also Baiesi & Paczuski 2004). It has been successfully applied to Italy for declustering (e.g. Essing & Poli 2024), its power relying in the capability to preserve the characteristics of the inhomogeneous and potentially non-stationary background seismicity. Differently from the window-based methods, that create notable gaps in declustered catalogues following major events because all the earthquakes inside a space–time window are removed from the catalogue (Peresan & Gentili 2020), the NN method merges the spatial and temporal distances between events in the same parameter. Therefore, a very small distance between events may compensate for a large temporal distance, merging together different clusters (Gentili *et al.* 2024).

A consistency between probabilistic and deterministic declustering approaches is valuable in PSHA context, where the deterministic declustering methods are applied, despite the problem they have with the Gutenberg–Richter *b*-value estimation (Mizrahi *et al.* 2021). The similarity of the methods justifies the use of the deterministic ones in PSHA, with the correction for *b*-value estimation suggested by Marzocchi & Taroni (2014).

The message we want to convey is that there is no general rule for one approach being preferable to the other, but it is essential to be aware of the meaning behind the selected approach and the implications it entails, to correctly interpret the results obtained.

ACKNOWLEDGMENTS

Funded by Seismic Hazard Center – WP3 Short-Term Probabilistic Seismic Hazard (CPS, Istituto Nazionale di Geofisica e Vulcanologia, NGV). Developed within the Bilateral project Italy–Japan - funded by the Italian Ministry of Foreign Affairs and International Cooperation, and the grant "Progetto INGV Pianeta Dinamico: NEar real-tiME results of Physical and StatIstical Seismology for earthquakes observations, modelling and forecasting (NEMESIS)" - code CUP D53J19000170001 - funded by Italian Ministry MIUR ("Fondo Finalizzato al rilancio degli investimenti delle amministrazioni centrali dello Stato e allo sviluppo del Paese", legge 145/2018). We also thank very much Dr. Ian Main, Dr. Piero Poli and an anonymous reviewer for their valuable comments and suggestions.

SUPPORTING INFORMATION

Supplementary data are available at *GJIRAS* online.

SupplementalMaterial.pdf

Please note: Oxford University Press is not responsible for the content or functionality of any supporting materials supplied by the authors. Any queries (other than missing material) should be directed to the corresponding author for the paper.

DATA AVAILABILITY

All data used in this paper came from the public source http://terremoti.ingv.it/ISIDe. Analysis were made using the MATLAB software. Codes and data can be shared after reasonable request to the corresponding author. This paper also contains a Supplemental Material, in which we report the Tables concerning the main information of the ULG- and the GK-clusters with the strongest magnitude ML $\geq$ 4.5, and some additional figures showing the results that expand at a greater detail some analyses discussed in the paper.

REFERENCES

Baiesi, M. & Paczuski, M., 2004. Scale-free networks of earthquakes and aftershocks, *Phys. Rev. E,* **69,** 066106.

Bayliss, K., Naylor, M. & Main, I. G., 2019. Probabilistic identification of earthquake clusters using rescaled nearest neighbour distance networks, *Geophys. J. Int.,* **217**(1), 487–503.

Benali, A., Jalilian, A., Peresan, A., Varini, E. & Idrissou, S., 2023. Spatiotemporal Analysis of the Background Seismicity Identified by Different Declustering Methods in Northern Algeria and Its Vicinity, *Axioms,* **12**(3). doi:10.3390/axioms12030237.

Console, R. & Murru, M., 2001. A simple and testable model for earthquake clustering, *J. Geophys. Res.: Solid Earth,* **106**(B5), 8699–8711.

Console, R., Murru, M. & Lombardi, A. M., 2003. Refining earthquake clustering models, *J. Geophys. Res.: Solid Earth,* **108**(B10), 2468.

Console, R., Murru, M., Catalli, F. & Falcone, G., 2007. Real Time Forecasts through an Earthquake Clustering Model Constrained by the Rate-and-State Constitutive Law: Comparison with a Purely Stochastic ETAS Model, *Seismol. Res. Lett.,* **78**(1), 49–56.

Console, R., Jackson, D. D. & Kagan, Y. Y., 2010. Using the ETAS model for catalog declustering and seismic background assessment, *Pure appl. Geophys.,* **167,** 819–830.

Essing, D. & Poli, P., 2024. Unraveling Earthquake Clusters Composing the 2014 Alto Tiberina Earthquake Swarm via Unsupervised Learning, *J. Geophys. Res.: Solid Earth,* **129**(1), e2022JB026237.

Gardner, J. K. & Knopoff, L., 1974. Is the sequence of earthquakes in Southern California, with aftershocks removed, Poissonian?, *Bull. seism. Soc. Am.,* **64**(5), 1363–1367.

Gentili, S. & Di Giovambattista, R., 2017. Pattern recognition approach to the subsequent event of damaging earthquakes in Italy, *Phys. Earth planet. Inter.,* **266,** 1–17.

Gentili, S., Brondi, P. & Di Giovambattista, R., 2023. NESTOREv1.0: A MATLAB Package for Strong Forthcoming Earthquake Forecasting, *Seismol. Res. Lett.,* **94**(4), 2003–2013.

Gentili, S., Brondi, P., Rossi, G., Sugan, M., Petrillo, G., Zhuang, J. & Campanella, S., 2024. Seismic clusters and fluids diffusion: a lesson from

the 2018 Molise (Southern Italy) earthquake sequence, *Earth, Planets and Space,* **76,** 157.
Gerstenberger, M. C. *et al.*, 2023. The 2022 Aotearoa New Zealand National Seismic Hazard Model: Process, Overview, and Results, *Bull. seism. Soc. Am.,* **114**(1), 7–36.
Gutenberg, B. & Richter, C. F., 1944. Frequency of earthquakes in California, *Bull. seism. Soc. Am.,* **34**(4), 185–188.
Herrmann, M. & Marzocchi, W., 2021. Inconsistencies and lurking pitfalls in the magnitude-frequency distribution of high-resolution earthquake catalogs, *Seismol. Res. Lett.,* **92**(2A), 909–922.
Keilis-Borok, V. I., Knopoff, L., Rotvain, I. M. & Sidorenko, T. M., 1980. Bursts of seismicity as long-term precursors of strong earthquakes, *J. Geophys. Res.: Solid Earth,* **85**(B2), 803–811.
Lolli, B. & Gasperini, P., 2003. Aftershocks hazard in Italy Part I: Estimation of time-magnitude distribution model parameters and computation of probabilities of occurrence, *J. Seismol.,* **7,** 235–257.
Lombardi, A. M. & Marzocchi, W., 2010. The ETAS model for daily forecasting of Italian seismicity in the CSEP experiment, *Ann. Geophys.,* **53**(3), 155–164.
Marzocchi, W. & Taroni, M., 2014. Some Thoughts on Declustering in Probabilistic Seismic-Hazard Analysis, *Bull. seism. Soc. Am.,* **104**(4), 1838–1845.
Marzocchi, W., Spassiani, I., Stallone, A. & Taroni, M., 2020. How to be fooled searching for significant variations of the b-value, *Geophys. J. Int.,* **220**(3), 1845–1856.
Mizrahi, L., Nandan, S. & Wiemer, S., 2021. The Effect of Declustering on the Size Distribution of Mainshocks, *Seismol. Res. Lett.,* **92**(4), 2333–2342.
Moretti, M., De Gori, P., Govoni, A., Margheriti, L., Piccinini, D., Pintore, S. & Valoroso, L., 2018. *Seismic data acquired by the SISMIKO emergency group–Molise-Italy 2018–T14 [Dataset],* Istituto Nazionale di Geofisica e Vulcanologia(INGV).
Nas, M., Jalilian, A. & Bayrak, Y., 2019. Spatiotemporal comparison of declustered catalogs of earthquakes in turkey, *Pure appl. Geophys.,* **176,** 2215–2233.
Ogata, Y., 1988. Statistical Models for Earthquake Occurrences and Residual Analysis for Point Processes, *J. Am. Stat. Assoc.,* **83**(401), 9–27.
Ogata, Y., 1998. Space-time point-process models for earthquake occurrences, *Ann. Inst. Stat. Math.,* **50,** 379–402.
Omi, T., Ogata, Y., Hirata, Y. & Aihara, K., 2014. Estimating the ETAS model from an early aftershock sequence, *Geophys. Res. Lett.,* **41**(3), 850–857.
Omori, F., 1895. On the aftershocks of earthquakes, *J. Coll. Sci., Imp. Univ., Jap.,* **7,** 111–200.
Peresan, A. & Gentili, S., 2020. Identification and characterization of earthquake clusters: a comparative analysis for selected sequences in Italy and adjacent regions, *Boll. Geofis. Teor. Appl.,* **61**(1), 57–80.
Rousseeuw, P. J. & Van Zomeren, B. C., 1990. Unmasking multivariate outliers and leverage points, *J. Am. Stat. Assoc.,* **85**(411), 633–639.
Scognamiglio, L. *et al.*, 2012. The 2012 Pianura Padana Emiliana seimic sequence: locations, moment tensors and magnitudes, *Ann. Geophys.,* **55**(4), 549–559.
Spassiani, I. & Marzocchi, W., 2018. How Likely Does an Aftershock Sequence Conform to a Single Omori Law Behavior?, *Seismol. Res. Lett.,* **89**(3), 1118–1128.
Talbi, A., Nanjo, K., Satake, K., Zhuang, J. & Hamdache, M., 2013. Comparison of seismicity declustering methods using a probabilistic measure of clustering, *J. Seismol.,* **17,** 1041–1061.
Tavani, F. & Spassiani, I., 2023. Detecting communities and complex network features of the italian earthquake catalog, in *AGU Fall Meeting Abstracts,* Vol. **2023,** pp. S33I–0496.
Uhrhammer, R. A., 1986. Characteristics of northern and central California seismicity, *Earthq. Notes,* **57**(1), 21.
Utsu, T., 1957. Magnitude of earthquakes and occurrence of their aftershocks, *Zisin,* **10,** 6–23 (in Japanese with English summary).
van Stiphout, T., Zhuang, J. & Marsan, D., 2012. Seismicity declustering, *Community Online Resource for Statistical Seismicity Analysis*. https://www.corssa.org/en/home/ (accessed April 2024).
Varini, E., Peresan, A. & Zhuang, J., 2020. Topological Comparison Between the Stochastic and the Nearest-Neighbor Earthquake Declustering Methods Through Network Analysis, *J. Geophys. Res.: Solid Earth,* **125**(8), e2020JB019718.
Zaliapin, I. & Ben-Zion, Y., 2013. Earthquake clusters in southern California II: Classification and relation to physical properties of the crust, *J. Geophys. Res.: Solid Earth,* **118**(6), 2865–2877.
Zaliapin, I., Gabrielov, A., Keilis-Borok, V. & Wong, H., 2008. Clustering analysis of seismicity and aftershock identification, *Phys. Rev. Lett.,* **101,** 018 501.
Zhuang, J., Ogata, Y. & Vere-Jones, D., 2002. Stochastic declustering of space-time earthquake occurrences, *J. Am. Stat. Assoc.,* **97**(458), 369–380.
Zhuang, J., Murru, M., Falcone, G. & Guo, Y., 2019. An extensive study of clustering features of seismicity in Italy from 2005 to 2016, *Geophys. J. Int.,* **216**(1), 302–318.

APPENDIX A: SPATIOTEMPORAL EQUATIONS DEFINING THE TWO WINDOW-BASED CLUSTERING APPROACHES

The two specific sets of equations we consider here to identify the clusters are the following:

(i) The law by Uhrhammer (1986) for space and the law by Lolli & Gasperini (2003) for time, as successfully applied in Italy by Gentili & Di Giovambattista (2017):

$$d = e^{0.804 \cdot M_{\mathrm{m}} - 1.024},$$
$$t = 60 + 60(M_{\mathrm{m}} - 4). \tag{A1}$$

We named this set of clusters "ULG-clusters".

(ii) The widely known equations by Gardner & Knopoff (1974), according to which the functional form of the spatiotemporal windows is obtained as:

$$d = 10^{0.1238 \cdot M_{\mathrm{m}} + 0.983},$$
$$t = 10^{A \cdot M_{\mathrm{m}} + B}, \tag{A2}$$

where

$$A = 0.032, \quad B = 2.7389 \quad if \quad M_{\mathrm{m}} \geq 6.5;$$
$$A = 0.5409, \quad B = -0.547 \quad if \quad M_{\mathrm{m}} < 6.5.$$

We named this set of clusters "GK-clusters".

In both cases, M_{m} is the mainshock magnitude, t is expressed in days, and d is in kilometers. Fig. S2 of the Supplemental Material gives a graphical comparison of the sets of eqs (A1) and (A2).

APPENDIX B: LARGEST ULG- AND GK-CLUSTERS AND THEIR COMPARISON

As explained in Section 4.2.3, we identified six ULG-clusters and seven GK-clusters with the strongest magnitude ML $\geq$ 5.0 ("*strongest*-ULG" and "*strongest*-GK" clusters, respectively). They are listed below:

(i) ML 5.2 (M_w 4.9) in Neviano degli Arduini (Parma province, Emilia-Romagna region), 2008 December 23 sequence, corresponding to the ULG cluster ID 9 and GK cluster ID 14, this latter being about five months longer than the former one.

(ii) L'Aquila sequence (Abruzzo region), 2009; strongest event on 2009 April 06 with ML 5.9 (M_w 6.1); this sequence is in ULG

cluster ID 10 and GK cluster ID 15, the latter being about eight months longer than the former (ULG-)one.

(iii) Emilia sequence (Northern Italy, Emilia–Romagna region), 2012; strongest events on 2012 May 20 with ML 5.9 (M_w 5.8), and on 2012 May 29 with ML 5.8 (M_w 5.6), this latter followed a few hours later by another strong event with ML 5.3 (M_w 5.3); in the case of ULG, this sequence is contained in a "single" cluster with ID 34, while the GK procedure split this sequence into two clusters with ID 35 (containing the ML 5.3 event), and ID 39 (containing the ML 5.9 and ML 5.8 events).

(iv) ML 5.2 (M_w 5.1) in Carrara (Massa-Carrara province, Toscana region), 2013 June 21; this sequence is in ULG cluster ID 43 and GK cluster ID 49, the latter being about 1 month longer than the former one;

(v) Central Italy sequence (Lazio, Abruzzo, Toscana, Umbria and Marche regions involved), 2016; strongest events on 2016 August 24 with ML 6.0 (M_w 6.0), and on 2016 October 30 with ML 6.1 (M_w 6.5); other strong events on 2016 October 26 with ML 5.9 (M_w 5.9) and on 2017 January 18 with ML 5.4 (M_w 5.5); this sequence is in ULG cluster ID 60 and GK cluster ID 66, the latter being about 1 yr longer than the former (ULG-)one;

(vi) ML 5.2 (M_w 5.1) in Montecilfone (Campobasso province, Molise region), 2018 August 16; this event is in ULG cluster ID 67 and GK cluster ID 70, the latter being about 1.5 months longer than the former.

The seismic map and referenced ID are given in the Supplemental Material (Fig. S9, Tables S1 and S3).